The future is fully defined: recombinant fragment E8 of laminin-511 is a viable xenofree alternative to Matrigel for hiPSC culture and differentiation into neurovascular cell types

Laís A. Ferreira, MSc[1,2]; Denise Fabiano do Nascimento[2]; Dr. Ishita Tandon[2]; Lance Cordes[2]; Dr. Kartik Balachandran[1,2*]

[1]Cellular & Molecular Biology Graduate Program, University of Arkansas, Fayetteville, Arkansas, United States of America

[2]Department of Biomedical Engineering, University of Arkansas Fayetteville, Arkansas, United States of America

*Corresponding author

E-mail: kbalacha@uark.edu (KB)

Abstract

Matrigel remains the gold standard substrate for culture of induced pluripotent stem cells (iPSCs). However, its highly variable composition, animal origin and unpredictable effects on biological activity have been discussed for more than 3 decades. In this study, we explore the use of fragment E8 of recombinant laminin 511, commercially available in form of iMatrix-511, as an alternative to Matrigel for iPSC maintenance and differentiation. Female iMR90-4 human iPSCs were cultured on either iMatrix or Matrigel and assessed for cell growth and viability, pluripotency, genetic stability, and ability to differentiate into isogenic brain microvascular endothelial cells (iBMECs) and brain pericytes. It was observed that iMatrix facilitated iPSC growth and viability comparable to Matrigel while maintaining a higher number of more consistently sized colonies. Additionally, like Matrigel, iMatrix maintained the expression of pluripotency markers SSEA-4 and OCT-3/4 over 15 passages without inducing DNA damage. iMatrix also supported the differentiation of these iPSCs into isogenic iBMECs and pericytes, which were successfully co-culture for generation of a simplified blood-brain barrier model. Overall, we showed that iMatrix, which is a cost effective, fully defined, and xenofree alternative can be used as a substitute for Matrigel for maintenance and differentiation of iPSCs.

Introduction

From layers of inactivated feeder cells [1] to humanized recombinant fragments of extracellular matrix (ECM) proteins with enhanced adhesion properties [2], the optimization of products and protocols for maintenance of induced pluripotent stem cells (iPSCs) in vitro is undeniably remarkable. With the constantly increasing interest in the study of iPSCs for therapeutic applications and disease modeling, various adhesion molecules and nutrient media

39 compositions have been developed and validated, some in fully defined and xenofree formulations,
40 contributing to overall better experimental reproducibility and robustness [3]. Currently, Matrigel
41 (MG) is the most widely used ECM for iPSC culture, evidencing its broad applicability. However,
42 this laminin-rich basement membrane preparation is secreted by mouse sarcoma cells, and
43 therefore highly variable in composition and animal derived. In fact, the need to cautiously
44 interpret data obtained from cells cultured on MG due to the biological activity of its undefined
45 and variable components have been discussed since 1992 [4,5].

46 Considering that laminins, which are the major component of MG, play an essential role
47 in the embryonic stem cell niche in vivo [6,7], the compatibility of several isoforms of laminin
48 with pluripotent stem cell culture have been investigated based on the integrins expressed by these
49 cells. In 2008, Miyazaki et al., pointed to the potential of human recombinant laminin-511 (LN511)
50 as a suitable substrate for undifferentiated expansion of human embryonic stem cells, which was
51 further confirmed by Rodin et al., 2010 and shown to promote superior cell adhesion than MG and
52 other laminins while maintaining pluripotency and normal karyotypes [7,8]. A few years later,
53 Miyazaki's research on recombinant laminins led to the isolation of fragment E8 of LN511
54 (LN511-E8), the active integrin-binding site, and demonstration of its superior affinity to human
55 pluripotent stem cells compared to its full-length counterpart [2].

56 Now, LN511-E8 is commercially available as iMatrix-511 (iM), a fully defined and
57 xenofree product for efficient maintenance of pluripotent stem cells in vitro. In addition to the
58 enhanced reproducibility resulting from the replacement of a poorly defined ECM mixture with a
59 purified truncated recombinant protein, iM features other important advantages to known MG
60 limitations, such as stability at room temperature, ease of manipulation, and improved cost
61 effectiveness [4]. Another major benefit of iM adoption for stem cell research compared with other

62 available products is that it allows for incorporation to the cell suspension immediately before
63 seeding, making the laborious and time-consuming pre-coating step expendable and cell culture
64 protocols substantially more flexible [9].

65 In this study, we aimed to investigate whether iM could be used as an alternative to MG in
66 a set of previously validated protocols for maintenance and differentiation of human iPSCs into
67 relevant cell types for blood-brain barrier (BBB) modeling. As hypothesized, based on previous
68 research and the fact that laminins account for approximately 60% of MG composition [4], our
69 results demonstrate that LN511-E8 efficiently supports iPSC culture while maintaining cell
70 growth, pluripotency, and genetic stability comparable to their counterparts cultured on MG. As
71 we delved deeper into the potential of these cells for tissue engineering applications, we have also
72 demonstrated that iM could be successfully adopted in protocols validated using MG for directed
73 differentiation into isogenic brain microvascular endothelial cells and brain pericytes. Overall, this
74 study offers valuable insights into the potential adaptability of protocols for pluripotent stem cells
75 research to increase experimental planning flexibility and facilitate compatibility with xenofree
76 and fully defined approaches.

77 Materials and methods

78 Details on cell culture reagents and primary antibodies used were included on S1 and S2 Tables,
79 respectively.

80 iPSC culture and coating strategies

81 A diagram illustrating the experimental design adopted in this study can be found in Fig 1.
82 The cell line used was the female iMR90-4, purchased from WiCell. iPSCs were fed mTeSR+
83 media daily and passaged when approximately 80% confluency was observed. Upon first seeding
84 after thawing, 10 mm Y-27632 (ROCK inhibitor) was added to the culture media – which was

removed 24 hours later. For comparative assessment of coating strategies one vial of cryopreserved cells was split into iM and growth factor reduced MG cultures and carried out in parallel, as shown in Fig 1. These cultures will be referred to as iM-iPSCs and MG-iPSCs, respectively. Three pairs of cultures were used in independent experiments for collection of the presented data. iM was used at 0.25 μg/cm^2 and added directly to the cell suspension immediately before seeding [9], while MG plates were pre-coated at 8.7 μg/cm^2 [10] in DMEM/F-12 media at 37°C at least overnight and up to 10 days before cell seeding. Both cultures were passaged using ReLeSR for maintenance and seeded on 25 mm Thermanox coverslips (Electron Microscopy Sciences) every odd passage, from P35 to P49, for identification of pluripotency markers octamer binding transcription factor-3/4 (OCT-3/4) [11] and the ganglioside stage-specific embryonic antigen-4 (SSEA-4) [12] through ICC techniques as described below.

Fig 1. Overview of the experimental design adopted in the study. Three pairs of cultures derived from the same initial cryovial were carried out in parallel using iMatrix or Matrigel. Undifferentiated iPSCs in passages between 37 and 38 were used for comparative assessment of cell growth and viability through daily cell counts and MTS assays, respectively. In every odd passage between 35 and 49, iPSCs were seeded on Thermanox coverslips for the identification of expression of the pluripotency markers SSEA-4 and OCT-3/4 through ICC techniques, and protein samples were collected for assessment of γH2AX expression as an indicator of genetic stability. iPSCs grown using iM and MG were differentiated into iBMECs and iPericytes using the equivalent ECM when appropriate and used to establish neurovascular co-cultures of cells generated using each strategy. Finally, the development of barrier phenotypes was comparatively assessed through TEER, permeability to a small molecule, and expression of the tight junction proteins claudin-5 and zonula occludens-1 (ZO-1). iBMECs: iPSC-derived brain microvascular endothelial cells; ICC: immunocytochemistry; iM: iMatrix; MG: Matrigel; OCT-3/4: octamer binding transcription factor-3/4; P: passage; SSEA-4: stage-specific embryonic antigen-4; TEER: transendothelial electrical resistance; TJ: tight junction. Created with BioRender.

110 ## Cell growth and viability assessment

111 For the analysis of cell growth, cells between P37 and P38 were lifted using ReLeSR and
112 seeded onto 24-well plates at a density of $2x10^4$ cells/cm^2 [9] in mTeSR+ following the coating
113 strategies described above. In each of the following four days, the typical interval between
114 passages, cells from two wells were imaged using an EVOS™ XL Core Imaging System, collected
115 following 6 min of incubation with accutase and counted using an automated cell counter
116 (Countess 3 FL, Thermo Fisher). Trypan blue was used to determine the number of live and dead
117 cells at each evaluated timepoint. Pictures taken 24h post seeding were used for colony attachment
118 analysis. Colonies were manually counted and measured using ImageJ (National Institutes of
119 Health, Bethesda, Maryland, USA). All colonies with an area greater than or equal to 1500 μm^2
120 were considered for colony size assessment. Data was collected from nine images per group
121 obtained in three independent experiments and reported as the average colony number and size per
122 image analyzed.

123 For further quantification of cell viability, MTS assays were also performed using cultures
124 between P37 and P38 according to the manufacturer instructions. In this case, $6.2x10^4$ cells/cm^2
125 were seeded onto 96-well plates [13] in quadruplicates for each period in culture to be assessed.
126 On the set timepoints, 20 µL of MTS was added to the wells containing 200 µL of cell culture
127 media. After 3h of incubation, media was transferred to a new 96-well plate for absorbance reading
128 at 490 nm. For every reading, wells containing only mTeSR+ and MTS (no cells) were also
129 included for normalization of the obtained values. In both assays media in the remaining wells was
130 changed daily until each experimental endpoint.

131 ## iPSC derived brain microvascular endothelial cells (iBMECs)

132 Differentiations into neurovascular cell types were started in parallel using iPSCs grown
133 on iM or MG and carried out using the same ECM in which initial undifferentiated cells were
134 previously cultured as shown in Fig 1. The differentiation of iPSCs into iBMECs was performed
135 based on a previously published method [14] summarized in Fig 5A and carried out in parallel
136 using iM (iM-iBMECs) or MG (MG-iBMECs) as described above. Briefly, on day 0, iPSCs were
137 incubated with accutase for 6 minutes at 37°C for singularization. Cells in suspension were
138 collected, sampled for counting, and centrifuged at 300g for 5 minutes. The supernatant was then
139 discarded, and the pellet was resuspended in mTeSR+ media containing 10 μM of ROCK inhibitor
140 to generate a cell suspension at a density of $1.2x10^5$ cells/mL. Cells were either seeded onto MG
141 pre-coated 6-well plates or uncoated plates after addition of iM to the suspension at a final density
142 of $12.5x10^3$ cells/cm^2.

143 On day 1 cells were given Essential 6 media (E6) to induce iBMEC differentiation, and
144 daily media changes were performed until day 4. From day 5 to 7, cells received endothelial cell
145 media (EC media), which consisted of human endothelial serum free medium supplemented with
146 B27, containing 20 ng/mL of FGF-2 and 10 μM of retinoic acid with no media change on day 6 –
147 characterizing the expansion phase. For further experimental use iBMECs were seeded onto 12
148 mm transwell inserts (Corning) and 15 mm Thermanox coverslips pre-coated with 0.4 mg/mL of
149 collagen IV and 0.1 mg/mL of fibronectin, which were prepared on day 6 to allow for overnight
150 incubation at 37°C. On day 7 the coating solution was aspirated, and plates were air dried for
151 approximately 20 min before cell seeding.

152 For subculturing, cells were incubated with accutase for 1h at 37°C to promote cell
153 detachment and singularization. Once in suspension, cells were collected, centrifuged in the above-
154 mentioned conditions, and resuspended in EC media containing 10 μM retinoic acid. iBMEC were

155 seeded based on a 1:3 split ratio, resulting in a density of approximately $2.5x10^6$ cells/transwell or
156 coverslip. After 24 hours, all media was replaced with EC media without retinoic acid. The success
157 of each differentiation process was assessed through the observation of expression of the tight
158 junction protein zonula occludens-1 (ZO-1) through ICC techniques and daily transendothelial
159 electrical resistance (TEER) measurements of cells seeded on coverslips and transwell inserts,
160 respectively, as described below.

161 iPSC derived brain pericytes (iPericytes)

162 Our protocol for the differentiation of iPSCs into brain pericytes (iPericytes), represented
163 on Fig 6A, was developed based on a previously published two-step method in which iPSCs are
164 initially differentiated into neural crest stem cells (iNCSC) before further differentiation into
165 iPericytes [15]. For that, on day 0 iPSCs were singularized and seeded as described above for
166 iBMEC differentiation, the only difference being a higher cell density of $9.1x10^4$ cells/cm^2. iNCSC
167 differentiation was induced on day 1, when media was switched to E6 supplemented with 1 μM
168 CHIR99021, 10 μM SB431542, 0.01 μg/mL FGF-2, 1 μM dorsomorphin, and 22.5 μg/mL heparin
169 – which will be referred to as E6-CSFD media. Cells were fed fresh E6-CSFD daily until day 15
170 and expanded in a 1:6 split ratio on days 3, 6, and 10 using accutase as previously described.
171 ROCK inhibitor was added to the cultures at a final concentration of 10 μM for 24 hours following
172 passaging on days 3 and 10 to increase cell attachment and viability at these critical time points of
173 the differentiation process. Until day 15, cells were cultured on MG pre-coated plates or had iM
174 added to cell suspensions immediately before seeding.

175 The first stage of the differentiation process was completed on day 15, when iNCSC
176 cultures were purified through magnetic cell sorting based on the expression of nerve growth factor
177 receptor (NGFR) according to manufacturer's instructions. After sorting, iNCSC were seeded

178 onto uncoated T-75 cell culture flasks (VWR) at a density of $1.4x10^4$ cells/cm^2. Thermanox
179 coverslips containing non-sorted iNCSCs were fixed with 4% paraformaldehyde (PFA; Electron
180 Microscopy Sciences) and NGFR expression was demonstrated through ICCs. Between days 16
181 and 25, cells were fed fresh E6 supplemented with 10% fetal bovine serum (FBS) daily, and one
182 passage was performed for expansion when cultures reached 90% confluency. For phenotype
183 confirmation, on day 25 fully differentiated iPericytes were fixed and the expression of cell
184 specific markers neural/glial antigen 2 (NG-2) and platelet-derived growth factor receptor β
185 (PDGFR-β) was assessed through ICCs.

186 Isogenic neurovascular co-culture

187 To comparatively assess the development of barrier phenotypes in neurovascular co-
188 cultures of iPSC-derived cells generated using iM or MG, on experimental day 0 iBMECs and
189 iPericytes differentiated on the same ECM were seeded onto the apical and basolateral chambers
190 of 12 mm transwells kept on 12 well-plates as shown in Fig 7A. A diagram summarizing the
191 timeline adopted for co-culture experiments can be found in Fig 7B. iPericytes were lifted from 75
192 cm^2 cell culture flasks using accutase and processed following the steps described above to be
193 seeded on the bottom of uncoated co-culture plates in E6 + 10% FBS at a density of $4.3x10^4$
194 cells/cm^2. Day 7 iBMECs were subcultured onto collagen/fibronectin-coated transwell inserts in
195 EC media + retinoic acid as previously detailed, which were then placed on iPericytes-seeded
196 wells. On day 1, media in all samples was refreshed and retinoic acid was removed from iBMECs
197 cultures. Thermanox coverslips, prepared according to cell type, were also included in every
198 experiment and cells were seeded separately at equivalent cell densities for confirmation of
199 iBMECs' and iPericytes' phenotypes through ICCs targeting ZO-1 and NG-2/PDGFR-β,
200 respectively, as described below.

201 # Barrier tightness assessment

202 The development of barrier phenotypes was measured via TEER and permeability to 3 kDa
203 dextran following the timeline shown in Fig 7B. An EVOM2 device (World Precision Instruments)
204 was used to measure TEER in iBMECs monocultures and co-cultures with iPericytes over 5 days.
205 Resistance was normalized through the subtraction of "blank" values collected from
206 collagen/fibronectin-coated transwells containing culture media only before cells were seeded on
207 day 0. For permeability assessment, 3kDa cascade blue-conjugated Dextran was diluted in EC
208 media at a final concentration of 100 µg/ml and added to apical chambers (Fig 7A) of co-cultures
209 on day 1. From day 2 to 5, 200 µl samples of E6 + 10% FBS were collected from the basolateral
210 chamber and replaced with the same volume of fresh media. Samples were stored at -20°C until
211 fluorescence intensity was measured using a Biotek Synergy Mix microplate reader at 400 ± 20
212 nm/450 ± 20 nm excitation/emission for determination of dextran concentrations in each sample.

213 For the establishment of a standard curve, dextran concentrations and the corresponding
214 fluorescence intensities were analyzed. Technical duplicates were averaged and normalized by the
215 subtraction of the baseline fluorescence intensity of the cell culture media in which samples were
216 collected. Values were graphed to find the standard fit curves using MATLAB 2023a with the
217 curve fitting toolbox add on. Using the fit function, the relationship between dextran
218 concentrations and fluorescence intensities were calculated using the custom equation $y = a(x^2)$
219 $+(b \times x)$ with y being the dextran concentration, x the fluorescence intensity, and a and b values
220 as the constants specific to each assay. After dextran concentrations were calculated, the
221 relationship between dextran concentration and the time points of each sample collection were
222 graphed. The slope $\frac{dC}{dt}$ was calculated from the graph using the slope equation $\frac{dC}{dt} = \frac{y2 - y1}{x2 - x1}$ and
223 adding a (0,0) point based on the assumption that the dextran concentration was 0 at time 0. The

224 obtained values were then used to calculate the apparent permeability (Papp) through the following
225 equation, where $Papp$ is the apparent permeability (cm/sec), Vr the sample volume collected (ml),
226 A the surface area of the porous membrane (cm^2), Co the initial concentration of dextran in the EC
227 media (mg/ml), and $\frac{dC}{dt}$ the slope of the dextran concentration over time (mg/(ml × sec)).
228

229 $$Papp = \frac{Vr}{A \times Co} \times \frac{dC}{dt}$$

230 # Immunocytochemistry (ICC)

231 Cells to be analyzed via ICC techniques for immunoidentification of targets of interest
232 were seeded on Thermanox coverslips – which were prepared following the same protocol used
233 for the maintenance of each cell type in culture. iPSC cultures were fixed with 4% PFA for 10 min,
234 while for iPSC-derived cells, PFA was added to the culture media at a 1% dilution and cells were
235 incubated for 2 min before exposure to 4% PFA for 8 min. Following fixation, iPSCs and iPSC-
236 derived cells were washed 3x with Phosphate-Buffered Saline (PBS) and Hank's Balanced Salt
237 Solution (HBSS), respectively, for 5 min under gentle orbital agitation. Blocking was performed
238 at room temperature for 1h using a PBS-based blocking buffer composed of 0.1% gelatin from
239 cold water fish skin (Sigma-Aldrich), 1% BSA, 2% normal goat serum (Thermo Fisher), 0.1%
240 Triton X-100 (Millipore-Sigma), and 0.05% Tween 20 (Amresco) [16,17]. Serum, Triton X-100,
241 and Tween-20 were not included in the blocking buffer for all markers and details on this step can
242 be found on S2 Table, as well as all primary antibodies used and respective dilutions. All primaries
243 were prepared in a solution of 1% BSA + 0.1% gelatin in PBS and allowed to bind to cellular
244 epitopes overnight at 4°C. AlexaFluor (ThermoFisher) goat anti-mouse and anti-rabbit 488 (green
245 fluorescence) and 594 (red fluorescence) were used as reporters at 1:100 and prepared in 1% BSA

246 with 1:200 DAPI (Thermo Fisher) for nuclear staining. Following 1h of incubation at room
247 temperature, coverslips were washed and mounted using ProLong Gold Antifade Mountant
248 between a 75x25x1 mm microscope slide (VWR) and a 50x24x0.16 mm cover glass (Fisher
249 Scientific) for image acquisition. Cells were imaged using an Olympus IX83 Inverted Confocal
250 Microscope and all obtained files were further processed using ImageJ for conversion into image
251 files and incorporation of scale bars.

252 Western blot

253 For collection of protein samples, iPSCs and iBMECs were washed 3x with cold PBS or
254 HBSS, respectively, for 5 min under gentle orbital agitation. Cells were lysed mechanically using
255 cell scrapers while exposed to RIPA buffer containing a cocktail of protease inhibitors, sodium
256 orthovanadate, and PMSF. Samples were then collected and centrifuged at 13,000 rpm for 10 min
257 at 4°C for isolation of supernatants and removal of cell debris. Total protein content in cell lysates
258 was determined using the Pierce Micro BCA Protein Assay Kit for normalization of protein
259 loading concentration for electrophoresis. Samples collected from undifferentiated iPSCs every
260 odd passage from 35 to 49 were loaded onto 4–20% Criterion TGX Precast Protein Gels (Bio-Rad)
261 at a total protein concentration of 50 µg. SDS-PAGE was performed at 200V for 50 min at 4°C on
262 ice. Proteins were then transferred to 0.45 µm pore size Immobilon-FL PVDF membranes
263 (Millipore-Sigma) using a wet tank system at 10V for 16h at 4°C that included a cooling pack and
264 a magnetic stir plate under constant agitation to keep the system from heating up. Membranes were
265 stained with Ponceau S (Sigma-Aldrich) for 10 min to allow for visualization of proteins and
266 assessment of transfer success. Blocking was carried out for 1h using Intercept (PBS) Protein-Free
267 Blocking Buffer (Li-Cor) before membranes were incubated with anti- γH2AX overnight at 4°C
268 for the assessment of DNA damage accumulation over 15 passages in culture.

269 Protein samples were also isolated from iBMECs grown on transwell inserts in co-culture
270 with iPericytes following the steps described above and 40 μg of total protein extract were
271 separated by molecular weight using 10% Criterion TGX Precast Protein Gels (Bio-Rad). In this
272 case transfers were carried out at 80V for 1.5h and membranes were also blocked for 1h before
273 incubation with primary antibodies targeting tight junction proteins claudin-5 and ZO-1. Blots
274 were imaged using an Odyssey Imager (Li-Cor) following labeling with fluorophore-conjugated
275 IRDye® 700CW and 800CW (Li-Cor) secondary antibodies. Densitometric analysis for protein
276 expression quantification was performed using ImageJ and GAPDH densitometry values were
277 used for signal normalization. For determination of the lane normalization factor, the value
278 corresponding to the signal intensity of GAPDH for each sample was divided by the highest
279 GAPDH signal on the blot. Data is presented as relative target protein signal, which was calculated
280 by dividing the signal intensity by the lane normalization factor.

281 Statistical analysis

282 All data sets were obtained from three experiments performed independently. GraphPad Prism
283 version 10.1.1 for Mac OS (GraphPad Software, Boston, Massachusetts USA) was used to assess
284 statistical significance and plot all graphs for data visualization. Data distribution was analyzed
285 through Shapiro-Wilk and proper statistical tests were defined accordingly. Details on sample sizes
286 and statistical tests corresponding to each data set are described on Fig captions. Differences were
287 considered significant if $p \leq 0.05$.

288 Results

289 iM facilitates the formation of a higher number of more consistent
290 sized colonies of iPSCs

291 For a comparative assessment of colony attachment patterns and cell proliferation in iPSCs
292 grown using iM and MG, cells were seeded onto 24-well plates at a density of $2x10^4$ cells/cm^2 and
293 in the following four days, the typical interval between passages for maintenance [3], phase
294 contrast images were obtained as well as cell counts. Analysis of images acquired 24h after seeding
295 (Fig 2A) showed that iM-iPSCs formed 42.75% more colonies than MG-iPSCs (p=0.0029), as
296 cells seeded using iM formed 127.8 ± 11.4 colonies compared to 82.8 ± 5.9 formed by their MG-
297 grown counterparts. When it comes to sizes, a trend towards larger colonies in MG-iPSCs was
298 observed, however with no significance (p=0.0907). Interestingly, when comparing the standard
299 error of the mean, the F test showed that colony sizes were more variable for MG-iPSCs than iM-
300 iPSCs (p=0.0265).

301 **Fig 2. Colony formation analyses.** Colony attachment was analyzed using **(A)** phase contrast microscopy images
302 taken 24h after cell seeding. Colonies were counted and outlined for determination of surface area using ImageJ. The
303 **(B)** number and **(C)** size of colonies are represented as Box & Whisker plots where the lines range from minimum to
304 maximum values and the boxes depict the lower to upper quartile. Data was collected from 9 fields of view imaged in
305 3 independent experiments for each group and statistical significance was assessed through unpaired t tests for both
306 datasets. **p=0.0029. ns: not significant.

307 The growth of iPSC colonies on both ECMs over four days can be visualized in the
308 representative phase contrast images included on Fig 3A. In each timepoint wells were gently
309 washed with D-PBS and the adhered cells were suspended and singularized using accutase for
310 quantification using an automated cell counter. The progression in total cell number for each group
311 over the assessed time in culture is shown in Fig 3B. Two-way ANOVA was adopted to
312 accommodate all relevant variables, which showed that days in culture was the only significant
313 source of variation for the evaluated data (p<0.0001), accounting for 69.3% of variation. The ECM
314 used was associated with 0.53% of variation (p=0.3995) and the interaction between both factors

315 for 0.37% (p=0.9184). Tukey's multiple comparisons post-hoc test was also performed and further
316 confirmed that the total cell number was statistically equivalent for iM-iPSCs and MG-iPSCs in
317 all timepoints assessed, although averaged counts were higher for iM-iPSCs from day 1 to 4. In
318 addition, both groups increased significantly in cell number over 4 days in culture in an equivalent
319 manner. On day 4, the number of iM-iPSCs and MG-iPSCs increased 10.7x (p<0.0001) and 11.3x
320 (p<0.0001), respectively, compared to data collected on day 1 – ranging from 94,490 ± 25,385 to
321 1,009,000 ± 150,811 for iM and 79,530 ± 22,538 to 899,333 ± 167,889 for MG.

322 **Fig 3. Growth and viability of iPSC cultures grown using iMatrix and Matrigel. (A)** Representative phase contrast
323 images of cells from both groups over four days in culture. Scale bars: 500 mm. The data from cell counts performed
324 daily is shown as **(B)** total cell counts and **(C)** the number of live and dead cells determined by an automated cell
325 counter based on trypan blue staining (n=6 counts/timepoint performed in 3 independent experiments). #percentage
326 of live cells in each timepoint for cells grown using iMatrix (top, orange) or Matrigel (bottom, green). Cell viability
327 was further assessed through **(D)** MTS assays (n=12 readings/timepoint performed in 3 independent experiments. All
328 data was analyzed through two-way ANOVAs followed by Tukey's multiple comparisons and is represented as mean
329 ± SEM. *p=0.0125; **p=0.0045; ***p=0.0003. ns: not significant.

330 iM supported similar increase in cell number to MG

331 With the incorporation of trypan blue in the cell counts described above, the number of live
332 and dead cells in each time point was also determined. As shown in Fig 3C, the number of both
333 live and dead cells was statistically equivalent for iM- and MG-iPSCs across all assessed
334 timepoints. Within each ECM, the number of dead cells remained constant for four days, while the
335 population of live cells progressively grew. The number of live cells increased significantly from
336 days 2 to 3 (p=0.0002 for iM and p=0.0192 for MG) and 3 to 4 (p=0.0066 for iM and p=0.0006
337 for MG) in both groups, which cumulatively led to a 10.6x increase in live iM-iPSCs (p<0.0001)

338 and 12x in MG-iPSCs ($p<0.0001$) from first to last count. The average percentage of live cells for
339 each day assessed was included in Fig 3C.

340 MTS assays were also performed and used as indicators of cell viability throughout 4 days
341 in culture. This colorimetric assay is based on the reduction of a tetrazolium compound into a
342 soluble colored formazan by metabolically active cells, which is proportional to the number of
343 viable cells and the absorbance values obtained [18,19]. As represented in Fig 3D, MG-iPSCs
344 showed significantly higher absorbance readings on days 2, 3, and 4. The most prominent
345 difference was observed on day 2, with a 55% difference between groups ($p=0.0003$), which
346 gradually decreased to 36% on day 3 ($p=0.0045$) and 29.4% on day 4 ($p=0.0125$). In contrast to
347 the observed for the number of viable cells within ECMs, there was a significant increase in
348 formazan conversion between days 1 and 2 ($p=0.0285$ for iM and $p<0.0001$ for MG) but no
349 difference between the subsequent days.

350

351 iM-iPSCs maintained pluripotency and genetic stability through 15 352 passages in culture

353 iMR90-4 iPSCs were thawed at P34 and grown up to P50 using either iM or MG. In all odd
354 passages within this range cells were fixed for immunostainings and protein samples were
355 collected. Fixed coverslips were used for phenotypic confirmation throughout 15 passages in
356 culture. Expression of pluripotency related markers SSEA-4 and OCT-3/4 was successfully
357 identified across passages for both iM- and MG-iPSCs. Representative images of cultures in P35
358 and P49, the first and last passages included in the study, are shown in Fig 4A and the complete
359 panel containing all passages evaluated can be found in S1 Fig. Protein samples were used for the
360 quantification of the phosphorylated form of histone H2AX (S139 γH2AX) through western blots.

361 γH2AX is formed as a response to DNA double strand breaks (DSB) and is commonly used as a
362 marker of DNA damage [20]. To establish a positive control, samples collected from iM-iPSCs in
363 P48 irradiated at 2.14 Gy/min totalizing 8 Gy were included in each experiment and the averaged
364 signal intensity of 12163.4 ± 4862.35 is represented by the red dotted line in Fig 4C. Šídák's
365 multiple comparisons test showed no statistical difference in γH2AX content in samples collected
366 from iM- and MG-iPSCs across all passages, which was also shown to be equivalent across
367 passages within each ECM through Tukey's post-hoc test (Fig 4C). In fact, analysis of variance
368 showed that ECM and passages accounted for only 5% (p=0.4057) and 14.5% (p=0.3285) of total
369 variation, respectively. The lowest and highest relative signal intensities were observed at P47
370 (3629 ± 1031) and P43 (8300 ± 1031) for iM-iPSCs, and P39 (5835 ± 2717) and P45 (10904 ±
371 3834) for MG-iPSCs. No correlation between passage and γH2AX content was found for cells
372 grown using either iM (p=0.2052, R^2=0.2517) or MG (p=0.2855, R^2=0.1864). The cumulative
373 γH2AX content was calculated as the average relative signal intensity for all samples in each ECM
374 and shown to be statistically equivalent (p=0.1251) between cells grown using iM (6356 ± 475.9)
375 or MG (7812 ± 801.2), although variance was significant larger in the MG group (p=0.0155).

376 **Fig 4. Pluripotency stability and DNA damage accumulation. (A)** Confocal microscopy images of iM- and MG-
377 iPSCs in passages 35 and 49 following immunolabeling of OCT-3/4 or SSEA-4 (red fluorescence) and nuclear staining
378 (blue fluorescence). Scale bars: 200 μM. **(B)** Representative images of western blot membranes used for densitometric
379 analysis to quantify γH2AX and GAPDH on protein samples obtained from 3 cultures of iM- and MG-iPSCs from
380 passage 35 to 49. **(C)** Relative signal intensity over passages is represented as mean ± SEM. The red line represents
381 mean signal intensity from irradiated iM-iPSCs. Statistical significance was assessed through two-way repeated
382 measures ANOVA followed by Šídák's and Tukey's multiple comparison tests to compare iM- and MG-iPSCs in
383 each passage and different passages within the same ECM group, respectively. n=3/passage/ECM. **(D)** Cumulative
384 γH2AX content is represented as a Box & Whisker plot where the lines range from minimum to maximum values and
385 the boxes depict the lower to upper quartile. Each point represents an individual measurement per passage, totalizing

n=24/ECM. Statistical significance was evaluated through an unpaired t test. ns: not significant. DAPI: 4′,6-diamidino-2-phenylindole; GAPDH: glyceraldehyde 3-phosphate dehydrogenase; OCT-3/4: octamer binding transcription factor-3/4; P: passage; SSEA-4: stage-specific embryonic antigen-4; γH2AX: phosphorylated H2A histone family member X.

iM supported directed differentiation of iPSCs into neurovascular cell types

iM- and MG-iPSCs were used to generate iBMECs and iPericytes following the equivalent ECM coating strategy according to the requirements of each differentiation protocol. Both target cell types were successfully generated using iM and MG, as shown in Figs 5 and 6. Images obtained after ZO-1 immunolabeling (Fig 5B) demonstrated that iM- and MG-iBMECs were capable of forming confluent monolayers and properly develop tight junctions. For further assessment of the development of barrier phenotypes by the iBMECs generated, TEER was measured over 5 days in culture. The obtained results revealed that resistance fluctuations followed a similar pattern for both cultures and no differences in average TEER was observed from day 1 to 4 after subculturing into transwell inserts, while statistical significance was found after 5 days in culture ($p=0.0142$, iM=54.88 ± 3.58 and MG=85.68 ± 7.03 $\Omega*cm^2$).

Normalized resistance peaked after 48h in culture for both groups, reaching 1161 ± 168.3 03 $\Omega*cm^2$ for iM-iBMECs and 1279 ± 213.8 03 $\Omega*cm^2$ for MG-iBMECs ($p=0.6738$). Peak TEER represented a 102.4% increase from 374.8 ± 43.49 $\Omega*cm^2$ on day 1 to 1161 ± 168.3 $\Omega*cm^2$ on day 2 for iM-iBMECs ($p=0.0119$), and a 116.5% increase from 337.3 ± 72.41 $\Omega*cm^2$ to 1279 ± 213.8 $\Omega*cm^2$ for their MG counterparts ($p=0.0282$). A similar trend was observed in the following drop in resistance from day 2 to 3. While iM-BMECs showed a 103% decrease to 371.5 ± 54.92 $\Omega*cm^2$

408 (p=0.0078), an 88.2% decrease to 496.3 ± 165.3 Ω*cm^2 (p=0.0064) was observed for MG-
409 iBMECs.

410 **Fig 5. Generation of human iPSC-derived brain microvascular endothelial cells. (A)** Schematic representation of
411 the differentiation timeline. **(B)** Confocal microscopy images of iBMECs following immunolabeling of ZO-1 (green
412 fluorescence) and nuclear staining (blue fluorescence). Scale bars: 200 μM. **(C)** Normalized TEER measurements
413 over 5 days, represented as mean ± SEM, for demonstration of successful iBMEC differentiation through the
414 quantification of barrier resistance. Statistical significance was assessed using a mixed effects model for repeated
415 measures followed by Tukey's multiple comparisons test. N=4-6 per time point measured in 3 independent
416 experiments. *p=0.0142, ns: not significant. DAPI: 4′,6-diamidino-2-phenylindole; iBMEC: iPSC-derived brain
417 microvascular endothelial cells; TEER: transendothelial electrical resistance; ZO-1: zonula occludens-1.

418 It has been suggested that although most peripheral pericytes have a mesodermal origin, neural
419 crest stem cells can be the developmental origin of the pericytes found in the central nervous
420 system, which can potentially entail important functional distinctions [21]. Therefore, a
421 methodological approach in which iPSCs are first differentiated into neural crest stem cells
422 (iNCSC) before being induced into iPericytes was adopted.

423 As shown by the expression of cell specific markers (Fig 6), we were able to successfully
424 differentiate iMR90-4 iPSCs into iNCSC and the latter into iPericytes using both matrices.
425 Projected Z-stacks of the immunoidentification of NGFR in non-sorted iNCSC showed extensive
426 expression of this marker across groups (Fig 6B), and on average the cell sorting process yielded
427 174,792 ± 14,941 and 168,958 ± 23,275 NGFR$^+$ cells per cm^2 collected for iNCSC generated using
428 iM and MG, respectively. An unpaired t test showed that the mean yield (p=0.8433) and variances
429 (p=0.5836) were statistically equivalent (n=3). Furthermore, acquisition of expression of NG-2
430 and PDGFR-β by NGFR$^+$ cells after 9 days of culture in E6 + 10% FBS on non-coated surfaces
431 demonstrates that fully differentiated iPericytes can be obtained through the proposed method
432 using either coating strategy (Fig 6C).

433 **Fig 6. Generation of human iPSC-derived brain pericytes. (A)** Schematic representation of the differentiation
434 timeline. **(B)** Confocal microscopy images of iNCSCs following immunolabeling of NGFR (red fluorescence) and
435 nuclear staining (blue fluorescence). **(C)** Confocal microscopy images of fully differentiated iPericytes following
436 immunolabeling of PDGFR-β (green fluorescence), NG-2 (red fluorescence), and nuclear staining (blue fluorescence).
437 Scale bars: 200 μM. DAPI: 4′,6-diamidino-2-phenylindole; E6-CSFD: Essential 6 media supplemented with
438 CHIR99021, SB431542, FGF-2, dorsomorphin, and heparin; FBS: fetal bovine serum; NG-2: neural/glial antigen 2;
439 NGFR: nerve growth factor receptor; PDGFR- β: platelet-derived growth factor receptor β.

440 One important drawback of the application of iPericytes for BBB modeling in this context, is
441 the length of the differentiation process. While iBMEC can be generated and seeded for
442 experimental analyses in 8 days, the differentiation of iPSCs into iPericytes is a 25-days long
443 process, as shown in the diagrams on Figs 5A and 6A. This factor hampers experimental planning
444 and requires that several simultaneous differentiation processes are performed to reduce the
445 interval between successive experimental rounds. Aiming to overcome this limitation, we
446 investigated the possibility to cryopreserve the cells in two different stages of differentiation.
447 Initially, iNCSC were frozen in serum free cell freezing media (Sigma) immediately after sorting
448 to take advantage of the addition of ROCK inhibitor to the cell culture media for 24 hours in this
449 step of the process. However, cells did not reattach when thawed in E6+20% FBS onto non-coated
450 cell culture plates.

451 The second approach tested was the cryopreservation of fully differentiated iPericytes after
452 day 25 in a freezing media composed of 50% E6, 40% FBS, and 10% dimethyl sulfoxide (DMSO;
453 Sigma) in the presence and absence of ROCK inhibitor. iPericytes were frozen at a density of
454 $1x10^6$ cells per cryovial and for thawing 1 vial was seeded onto a non-coated T-25 cell culture
455 flask (Corning) in E6+20% FBS, and the serum concentration was decreased to 10% after 24 hours.
456 In this case, cell recovery was successful after maintenance in liquid nitrogen, and more efficient
457 for cells frozen with ROCK inhibitor, which showed improved cell adhesion and survival in the

458 first 24 hours following seeding (S2 Fig B). Phenotyping of thawed cells demonstrated that the
459 expression of cell specific markers was retained after freezing (S2 Fig A). The successful
460 cryopreservation of iPericytes described here represents an important tool to enhance experimental
461 efficiency for human iPSC-based isogenic multicellular BBB modeling.

462 iM serves as a suitable substrate for generation of iPSC-derived cells 463 for BBB modeling

464 iBMECs and iPericytes were paired by ECM and co-cultured on a transwell system, as
465 demonstrated in Fig 7A, for a comparative assessment of their performance as a BBB model
466 following the experimental timeline shown in Fig 7B. Co-cultures were maintained for 5 days and
467 throughout this period TEER, permeability, and expression of tight junction proteins were
468 measured as indicators of development of barrier properties. When it comes to TEER, no
469 significant differences were observed between iM and MG co-cultures from day 1 to 5, as shown
470 in Fig 7C. Peak resistance was achieved 48h after seeding for co-cultures in both groups, reaching
471 1410 ± 91.67 $\Omega*cm^2$ for iM and 1265 ± 121.7 $\Omega*cm^2$ for MG, representing a 137% (p=0.0131)
472 and 118.5% (p=0.5656) increase from day 1, respectively. The decrease in TEER observed
473 between days 2 and 3 was not significant for either group (p=0.0666 for iM and p=0.1704 for MG).
474 After 5 days in culture, resistance significantly dropped compared to peak values for both iM
475 (p=0.0097) and MG (p=0.03) co-cultures.

476 Apparent permeability was also found to be statistically equivalent between iM- and MG-
477 derived co-cultures in all time points included in this study (Fig 7D). In a closer look, a significant
478 increase in permeability was observed between days 2 and 5 for both experimental groups. iM-
479 derived co-cultures showed a 10.5x increase in this period (p=0.0021), while for their MG
480 counterparts a 16.7x difference was observed (p=0.0439). Co-cultures generated using iM-derived

481 cells also showed significantly higher permeability on day 5 compared to days 3 (p=0.0081) and
482 4 (p=0.0054), while the same was not observed for MG-derived cells.

483 Finally, expression of tight junction proteins claudin-5 and ZO-1 was analyzed through
484 western blots (Fig 7E-G). On day 3, MG-iBMECs (9660 ± 1129) in co-culture showed
485 significantly higher expression of claudin-5 (p=0.0220) compared to iM-iBMECs (6204 ± 424.2).
486 Variance was also found to be higher for MG-iBMECs (p=0.0148) (Fig 7F). ZO-1 expression, on
487 the other hand, was equivalent between both groups (p=0.1640), although variance in this case
488 was significantly higher for iM-iBMECs (p=0.0002) (Fig 7G).

489 **Fig 7. Co-culture of isogenic iPSC-derived brain microvascular endothelial cells and brain pericytes. (A)**
490 Schematic representation of co-cultures on transwells, showing iBMECs on the apical chamber and iPericytes on the
491 basolateral chamber. **(B)** Representative diagram of the experimental timeline adopted for co-culture studies. **(C)**
492 Normalized TEER measurements over 5 days, represented as mean ± SEM. Statistical significance of averaged
493 replicates per time point was evaluated through two-way ANOVA followed by Tukey's multiple comparisons test.
494 N=6-9 per time point measured in 3 independent experiments. **(D)** Apparent permeability of iBMECs monolayers to
495 3 kDa dextran over 4 days in culture represented as mean ± SEM. Statistical significance was assessed using a mixed
496 effects model for repeated measures followed by Tukey's multiple comparisons test. N=4-6 per time point measured
497 in 3 independent experiments. **(E)** Expression of tight junction proteins was evaluated using western blots. Relative
498 signal intensity of **(F)** claudin-5 and **(G)** ZO-1 was determined through densitometric analysis using GAPDH
499 expression for normalization and plotted as mean ± SEM. Significance of mean differences was assessed through
500 unpaired t tests with a total n=7-9 for claudin-5 and n=5 for ZO-1 corresponding to samples collected in 3 independent
501 experiments. *p=0.022, ns: not significant. GAPDH: glyceraldehyde 3-phosphate dehydrogenase; iBMEC: iPSC-
502 derived brain microvascular endothelial cells; iM: iMatrix; MG: Matrigel; Papp: apparent permeability; RA: retinoic
503 acid; TEER: transendothelial electrical resistance; ZO-1: zonula occludens 1. A & B were created using BioRender.

504 # Discussion

505 This study investigated the use of iM, a commercially available recombinant fragment of
506 human laminin-511, as a xenofree and fully defined alternative to MG. While earlier studies have
507 demonstrated that the fragment E8 of laminin-511 (LN511-E8) supports maintenance and
508 differentiation of pluripotent stem cells in vitro [2,9,22,23], its use to reproduce methods validated
509 using MG have not been explicitly addressed. In this study, we have demonstrated that iM-iPSCs
510 behave similarly to MG-iPSCs and can be differentiated into neurovascular cell types using
511 protocols established using MG.

512 A key requirement of iPSC maintenance is that these cells require passaging in aggregates to
513 avoid myosin-actin contraction related cell death without the need to incorporate ROCK inhibitor
514 in routine expansion protocols. Ideally, aggregates should be consistent in size while large enough
515 to reattach as colonies and ensure cell survival and small enough to facilitate access by growth
516 factors and other small molecules [24,25]. Through colony attachment analysis, we found that 24h
517 after seeding iM-iPSCs are significantly less variable in size than MG-iPSCs and, although not
518 significantly, smaller considering the surface area covered. Consistently, more colonies were
519 formed upon attachment to iM, suggesting that iPSCs grown on iM reattach in more colonies that
520 are smaller in size compared to MG-cultured cells, which formed more and larger colonies. These
521 observations can be associated with the consistency of cell dissociation for expansion and the size
522 and number of aggregates generated as cells anchored to both matrices are released from the plate
523 and neighboring cells. Therefore, iM might be more compatible with aggregate passaging [4,24].
524 A previous study has also demonstrated that LN511-E8 support stronger adhesion of singularized
525 iPSCs than MG and even intact LN511, while making the addition of ROCK inhibitor optional
526 following complete dissociation and allowing for uniform cell seeding in defined densities [2].

527 When it comes to cell behavior in culture, we have demonstrated that the number of iM-iPSCs
528 and MG-iPSCs increased similarly in the typical interval between passages [3], showing stable
529 and consistent activation of DNA damage responses and retaining expression of pluripotency
530 markers across 15 passages. Interestingly, while the number of live and dead cells after trypan-
531 blue staining was statistically equivalent for iM and MG in all time points, MTS readings were
532 significantly higher for MG-iPSCs from day 2 to 4 after seeding. Note that, although not
533 significantly, live cell counts were higher for iM-iPSCs every day, with the smallest difference
534 coinciding with the higher difference in MTS readings on day 2. Interestingly, these two methods
535 rely on different cellular responses. While trypan blue allows for the identification of cells with
536 compromised membranes, the MTS assay detects differences in mitochondrial metabolism as the
537 reaction quantified is believed to be performed mainly by NAD(P)H-dependent oxidoreductases
538 [26,27].

539 In a study comparing four methods for determining viability of fibroblasts after irradiation with
540 increasing doses of blue light, statistical significance was first detected with a tetrazolium-based
541 assay (i.e. MTT) at 55 J/cm^2 and subsequently with MTT and trypan blue at 110 J/cm^2. The
542 reported data demonstrates that mitochondrial metabolism is affected before membrane integrity
543 is compromised, demonstrating that these methods differ in sensitivity [27]. In this case, the
544 difference we observed could be a result of reduced metabolic activity in iPSCs grown on iM that
545 did not reflect in membrane damage. On the other hand, there is evidence that metabolic
546 dysregulation may increase the flow of electrons to artificial dyes through compensatory reactions,
547 which can be mistaken by increased NAD(P)H available for cell proliferation [26]. Although the
548 effects of MG on iPSC metabolism have not yet been directly addressed, it has been shown that
549 its incorporation into the media for culture of breast cancer spheroids under hypoxia leads to

550 increased Nrf2 expression and nitric oxide levels, as well as decreased levels of glutathione
551 compared to cells kept in absence of MG, therefore attesting for a potential role of its bioactive
552 components in modulating cellular metabolism [28]. It is also important to take into account that
553 MG was prepared for surface coating in DMEM/F12 containing glucose, where its presence in
554 culture media has been shown to increase tetrazolium reduction in HEK293 and HeLa cells [29].
555 Overall, the obtained data suggests that iM supports iPSCs growth and survival similarly to MG.
556 These results also emphasize the need for future studies providing a closer look at possible effects
557 of MG in modulating mitochondrial metabolism given its major role in pluripotency maintenance
558 [30] and the importance of combining different viability assays for a better understanding of
559 cellular responses [27].

560 According to evidence showing that the full form of laminin-511 [8] and LN511-E8 [2,9]
561 support continuous subculture of pluripotent stem cells with normal karyotypes for up to 30
562 passages, our analysis of γH2AX content in cells grown on both matrices suggests that iM works
563 as well as MG when it comes to maintaining genetic stability across passages. Considered the most
564 sensitive marker for detection of DNA damage, γH2AX is the phosphorylated form of histone
565 H2AX, which is rapidly formed in response to DNA double-strand breaks [31]. It is important to
566 note that iPSCs show a higher basal level of γH2AX compared to somatic cell types, which has
567 been suggested to be associated with increased proliferation rates and shown to decrease in
568 differentiated progeny [32].

569 In addition to genetic stability, previous studies have demonstrated that LN511-E8 supports
570 long-term maintenance of undifferentiated iPSCs with steady expression of several pluripotency
571 markers [2,9,22], including SSEA-4 and OCT-3/4, which were also observed in cultures grown on
572 both iM and MG in every odd passage between 35 and 49 in this study. Tied to proper maintenance

573 of pluripotency is the ability of cells to respond properly to stimuli to differentiate into somatic
574 cell types – a critical step for most iPSCs applications. Several differentiation protocols are
575 performed using MG-coated surfaces, thus an efficient ECM alternative would ideally be
576 completely interchangeable, supporting targeted differentiation as well as undifferentiated
577 proliferation. It has been shown that iPSCs cultured on LN511-E8 can generate embryoid bodies
578 and teratomas expressing gene markers for all three germ layers [2,9,22] and undergo directed
579 differentiation into dopaminergic neurons, blood cells, and insulin-producing cells with LN511-
580 E8 being incorporated in steps that required ECM coating [22]. To complement what is known
581 about the compatibility of LN511-E8 with differentiation protocols, we have demonstrated that
582 methods previously validated using MG for the generation of iBMECs, iNCSCs, and iPericytes
583 [14,15] can be replicated using iM.

584 iPSC-derived cells are a powerful tool for disease modeling, impacting immensely the
585 physiological relevance of benchtop models based on their applicability for personalized medicine
586 and development of increasingly complex isogenic multicellular systems [33]. Therefore,
587 following successful generation of neurovascular cell types using iM and MG, isogenic iBMECs
588 and iPericytes generated using the same ECM were combined and co-cultured [15] for 5 days in a
589 transwell system for a comparative assessment of the development of barrier phenotypes.
590 Characterization of co-cultures of iPSC derived BMECs and pericytes and even BMEC
591 monocultures have shown that cellular behavior can differ substantially between studies, for
592 example reaching higher [34] and lower [15] TEER values than reported here, which is possibly a
593 consequence of significant variations in differentiation protocols and iPSC lines used. Nonetheless,
594 our results demonstrate that iBMECs generated using both strategies can form proper tight
595 junctions [34,35] and peak in resistance above 1000 $\Omega*cm^2$ after 48h in co-culture with iPericytes.

596 As expected, the highest apparent permeability coincided with the lowest TEER values on day 5
597 in both conditions, suggesting the loss of barrier integrity over time. Other studies have shown that
598 iPSC-derived BBB models can reach TEER values up to 4000 Ω*cm^2 [14,34]. Differences in
599 TEER numbers between these previous studies and our current work are possibly due to
600 differences in specific culture reagents used. However, as cells from both treatment groups were
601 manipulated simultaneously and exposed to the exact same conditions in each experiment, these
602 differences in TEER numbers from previous studies are not detrimental to a comparative analysis.
603 Finally, complementing the assessment of BBB-like phenotypes in endothelial cells, we have
604 demonstrated using a semiquantitative method that the expression of claudin-5 is upregulated in
605 MG-iBMECs compared to iM-iBMECs, while ZO-1 expression was statistically equivalent
606 between both groups despite a trend towards higher expression by iM-iBMECs. Proper formation
607 of tight junctions is essential for the establishment of inter-endothelial connections, which plays a
608 major role in BBB tightness and healthy function, controlling paracellular transport and barrier
609 permeability [36]. Several studies have previously demonstrated that iBMECs generated using MG
610 or vitronectin express cell junction proteins, such as VE-cadherin, occludin, claudin-5, and ZO-1
611 [14,15,34,37]. Claudin-5, the most enriched tight junction protein in the neurovasculature, is an
612 integral membrane protein that tightly connects adjacent cells, and its intracellular domains are
613 anchored to the actin cytoskeleton through scaffolding proteins such as ZO-1/2/3 [36]. Its role in
614 controlling barrier permeability is so important, that its selective modulation is being studied as a
615 pharmacological target to increase drug delivery to the brain and as a strategy to stabilize cellular
616 junctions to treat disorders associated with BBB leakage [38]. Similarly, it has been demonstrated
617 that cells lacking ZO proteins show disrupted tight junction formation, with claudins failing to
618 polymerize [39], hence the importance of demonstrating that iM- and MG-iBMECs express both

proteins. Taken together, the presented data suggests that although MG-iBMECs show higher claudin-5 expression, the observed difference did not result in functional changes in barrier tightness under evaluated conditions, as confirmed by statistically equivalent TEER and apparent permeability through 5 days in co-culture with iPericytes. In this case, if also taking into account the presence of known and unknown bioactive components in MG, the possibility of its effect on differences in gene and protein expression cannot be overlooked [4] and should be addressed in future studies.

Overall, our findings indicate that iM is a viable fully defined and xenofree alternative to MG for iPSC maintenance and differentiation into relevant cell types for neurovascular modeling, yielding similar results in the establishment of a simplified isogenic iPSC-derived BBB in vitro system. Ultimately, evidence presented here will contribute to increasing flexibility in the development of protocols for culture and targeted differentiation of pluripotent stem cells, while supporting the enhanced experimental robustness and reproducibility that comes with the adoption of fully defined and batch-to-batch consistent ECM products for cell culture.

Acknowledgments

The authors would like to thank the contributions of Dr. Young Hye Song and In Ha Baek (University of Arkansas), for providing training and access to their confocal microscope for acquisition of all ICC images included in this publication; and Dr. Rajaram and Dr. Whitney Ann Lowe (University of Arkansas) for enabling and assisting with the irradiation of iPSC cultures.

References

1. Thomson JA, Itskovitz-Eldor J, Shapiro SS, Waknitz MA, Swiergiel JJ, Marshall VS, et al. Embryonic Stem Cell Lines Derived from Human Blastocysts. Science [Internet]. 1998 Nov 6 [cited 2024 May 13];282(5391):1145–7. Available from: https://www.science.org/doi/10.1126/science.282.5391.1145

643 2. Miyazaki T, Futaki S, Suemori H, Taniguchi Y, Yamada M, Kawasaki M, et al. Laminin E8
644 fragments support efficient adhesion and expansion of dissociated human pluripotent stem
645 cells. Nat Commun [Internet]. 2012 Dec 4 [cited 2024 Apr 28];3(1):1236. Available from:
646 https://www.nature.com/articles/ncomms2231

647 3. Lyra-Leite DM, Gutiérrez-Gutiérrez Ó, Wang M, Zhou Y, Cyganek L, Burridge PW. A
648 review of protocols for human iPSC culture, cardiac differentiation, subtype-specification,
649 maturation, and direct reprogramming. STAR Protocols [Internet]. 2022 Sep [cited 2024
650 May 5];3(3):101560. Available from:
651 https://linkinghub.elsevier.com/retrieve/pii/S2666166722004403

652 4. Aisenbrey EA, Murphy WL. Synthetic alternatives to Matrigel. Nat Rev Mater [Internet].
653 2020 Jul [cited 2021 Nov 15];5(7):539–51. Available from:
654 http://www.nature.com/articles/s41578-020-0199-8

655 5. Vukicevic S, Kleinman HK, Luyten FP, Roberts AB, Roche NS, Reddi AH. Identification of
656 multiple active growth factors in basement membrane matrigel suggests caution in
657 interpretation of cellular activity related to extracellular matrix components. Experimental
658 Cell Research [Internet]. 1992 Sep 1 [cited 2024 May 3];202(1):1–8. Available from:
659 https://www.sciencedirect.com/science/article/pii/001448279290397Q

660 6. Kiyozumi D, Nakano I, Sato-Nishiuchi R, Tanaka S, Sekiguchi K. Laminin is the ECM niche
661 for trophoblast stem cells. Life Science Alliance [Internet]. 2020 Feb 1 [cited 2024 May
662 13];3(2). Available from: https://www.life-science-alliance.org/content/3/2/e201900515

663 7. Miyazaki T, Futaki S, Hasegawa K, Kawasaki M, Sanzen N, Hayashi M, et al. Recombinant
664 human laminin isoforms can support the undifferentiated growth of human embryonic stem
665 cells. Biochemical and Biophysical Research Communications [Internet]. 2008 Oct [cited
666 2024 May 13];375(1):27–32. Available from:
667 https://linkinghub.elsevier.com/retrieve/pii/S0006291X08014319

668 8. Rodin S, Domogatskaya A, Ström S, Hansson EM, Chien KR, Inzunza J, et al. Long-term
669 self-renewal of human pluripotent stem cells on human recombinant laminin-511. Nat
670 Biotechnol [Internet]. 2010 Jun [cited 2024 Apr 28];28(6):611–5. Available from:
671 https://www.nature.com/articles/nbt.1620

672 9. Miyazaki T, Isobe T, Nakatsuji N, Suemori H. Efficient Adhesion Culture of Human
673 Pluripotent Stem Cells Using Laminin Fragments in an Uncoated Manner. Sci Rep
674 [Internet]. 2017 Mar [cited 2021 Oct 14];7(1):41165. Available from:
675 http://www.nature.com/articles/srep41165

676 10. Kuo HH, Gao X, DeKeyser JM, Fetterman KA, Pinheiro EA, Weddle CJ, et al. Negligible-
677 Cost and Weekend-Free Chemically Defined Human iPSC Culture. Stem Cell Reports
678 [Internet]. 2020 Feb [cited 2023 Dec 9];14(2):256–70. Available from:
679 https://linkinghub.elsevier.com/retrieve/pii/S2213671119304461

680 11. Shi G, Jin Y. Role of Oct4 in maintaining and regaining stem cell pluripotency. Stem Cell
681 Research & Therapy [Internet]. 2010 Dec 14 [cited 2024 Feb 2];1(5):39. Available from:
682 https://doi.org/10.1186/scrt39

683 12. Virant-Klun I, Kenda-Suster N, Smrkolj S. Small putative NANOG, SOX2, and SSEA-4-
684 positive stem cells resembling very small embryonic-like stem cells in sections of ovarian
685 tissue in patients with ovarian cancer. J Ovarian Res [Internet]. 2016 Mar 3 [cited 2024 Feb
686 2];9:12. Available from: https://www.ncbi.nlm.nih.gov/pmc/articles/PMC4778328/

687 13. Ghasemi M, Turnbull T, Sebastian S, Kempson I. The MTT Assay: Utility, Limitations,
688 Pitfalls, and Interpretation in Bulk and Single-Cell Analysis. IJMS [Internet]. 2021 Nov 26
689 [cited 2023 Dec 9];22(23):12827. Available from: https://www.mdpi.com/1422-
690 0067/22/23/12827

691 14. Neal EH, Marinelli NA, Shi Y, McClatchey PM, Balotin KM, Gullett DR, et al. A
692 Simplified, Fully Defined Differentiation Scheme for Producing Blood-Brain Barrier
693 Endothelial Cells from Human iPSCs. Stem Cell Reports [Internet]. 2019 Jun [cited 2020
694 Aug 29];12(6):1380–8. Available from:
695 https://linkinghub.elsevier.com/retrieve/pii/S2213671119301754

696 15. Stebbins MJ, Gastfriend BD, Canfield SG, Lee MS, Richards D, Faubion MG, et al. Human
697 pluripotent stem cell–derived brain pericyte–like cells induce blood-brain barrier properties.
698 Sci Adv [Internet]. 2019 Mar 20 [cited 2021 Oct 14];5(3):eaau7375. Available from:
699 https://www.science.org/doi/10.1126/sciadv.aau7375

700 16. McCallinhart PE, Biwer LA, Clark OE, Isakson BE, Lilly B, Trask AJ. Myoendothelial
701 Junctions of Mature Coronary Vessels Express Notch Signaling Proteins. Front Physiol
702 [Internet]. 2020 Feb 4 [cited 2023 Dec 10];11:29. Available from:
703 https://www.frontiersin.org/article/10.3389/fphys.2020.00029/full

704 17. Piña R, Santos-Díaz AI, Orta-Salazar E, Aguilar-Vazquez AR, Mantellero CA, Acosta-
705 Galeana I, et al. Ten Approaches That Improve Immunostaining: A Review of the Latest
706 Advances for the Optimization of Immunofluorescence. IJMS [Internet]. 2022 Jan 26 [cited
707 2023 Dec 10];23(3):1426. Available from: https://www.mdpi.com/1422-0067/23/3/1426

708 18. Berridge MV, Herst PM, Tan AS. Tetrazolium dyes as tools in cell biology: New insights
709 into their cellular reduction. In: Biotechnology Annual Review [Internet]. Elsevier; 2005
710 [cited 2024 Jan 21]. p. 127–52. Available from:
711 https://linkinghub.elsevier.com/retrieve/pii/S1387265605110047

712 19. Stepanenko AA, Dmitrenko VV. Pitfalls of the MTT assay: Direct and off-target effects of
713 inhibitors can result in over/underestimation of cell viability. Gene [Internet]. 2015 Dec
714 [cited 2024 Jan 21];574(2):193–203. Available from:
715 https://linkinghub.elsevier.com/retrieve/pii/S037811191500952X

716 20. Mariotti LG, Pirovano G, Savage KI, Ghita M, Ottolenghi A, Prise KM, et al. Use of the γ-
717 H2AX Assay to Investigate DNA Repair Dynamics Following Multiple Radiation

718 Exposures. Robson CN, editor. PLoS ONE [Internet]. 2013 Nov 29 [cited 2024 Feb
719 2];8(11):e79541. Available from: https://dx.plos.org/10.1371/journal.pone.0079541

720 21. Jamieson JJ, Searson PC, Gerecht S. Engineering the human blood-brain barrier in vitro. J
721 Biol Eng [Internet]. 2017 Dec [cited 2022 Jul 31];11(1):37. Available from:
722 https://jbioleng.biomedcentral.com/articles/10.1186/s13036-017-0076-1

723 22. Nakagawa M, Taniguchi Y, Senda S, Takizawa N, Ichisaka T, Asano K, et al. A novel
724 efficient feeder-free culture system for the derivation of human induced pluripotent stem
725 cells. Sci Rep [Internet]. 2014 Jan 8 [cited 2024 Apr 28];4(1):3594. Available from:
726 https://www.nature.com/articles/srep03594

727 23. Nakashima Y, Tsukahara M. Laminin-511 Activates the Human Induced Pluripotent Stem
728 Cell Survival via α6β1 Integrin-Fyn-RhoA-ROCK Signaling. Stem Cells Dev [Internet].
729 2022 Nov 1 [cited 2024 Apr 30];31(21–22):706–19. Available from:
730 https://www.ncbi.nlm.nih.gov/pmc/articles/PMC9700348/

731 24. Beers J, Gulbranson DR, George N, Siniscalchi LI, Jones J, Thomson JA, et al. Passaging
732 and colony expansion of human pluripotent stem cells by enzyme-free dissociation in
733 chemically defined culture conditions. Nat Protoc [Internet]. 2012 Nov [cited 2024 Apr
734 26];7(11):2029–40. Available from: https://www.nature.com/articles/nprot.2012.130

735 25. Chen G, Hou Z, Gulbranson D, Thomson JA. Actin-myosin contractility is responsible for
736 the reduced viability of dissociated human embryonic stem cells. Cell Stem Cell [Internet].
737 2010 Aug 6 [cited 2024 Apr 26];7(2):240–8. Available from:
738 https://www.ncbi.nlm.nih.gov/pmc/articles/PMC2916864/

739 26. Aleshin VA, Artiukhov AV, Oppermann H, Kazantsev AV, Lukashev NV, Bunik VI.
740 Mitochondrial Impairment May Increase Cellular NAD(P)H: Resazurin Oxidoreductase
741 Activity, Perturbing the NAD(P)H-Based Viability Assays. Cells [Internet]. 2015 Aug 21
742 [cited 2024 Apr 29];4(3):427–51. Available from:
743 https://www.ncbi.nlm.nih.gov/pmc/articles/PMC4588044/

744 27. Masson-Meyers DS, Bumah VV, Enwemeka CS. A comparison of four methods for
745 determining viability in human dermal fibroblasts irradiated with blue light. Journal of
746 Pharmacological and Toxicological Methods [Internet]. 2016 May [cited 2024 Apr
747 29];79:15–22. Available from:
748 https://linkinghub.elsevier.com/retrieve/pii/S1056871916300016

749 28. Badea MA, Balas M, Hermenean A, Ciceu A, Herman H, Ionita D, et al. Influence of
750 Matrigel on Single- and Multiple-Spheroid Cultures in Breast Cancer Research. SLAS
751 Discovery [Internet]. 2019 Jun 1 [cited 2024 Apr 29];24(5):563–78. Available from:
752 https://www.sciencedirect.com/science/article/pii/S247255522206782X

753 29. Xie L, Dai Z, Pang C, Lin D, Zheng M. Cellular glucose metabolism is essential for the
754 reduction of cell-impermeable water-soluble tetrazolium (WST) dyes. Int J Biol Sci
755 [Internet]. 2018 Sep 7 [cited 2024 May 12];14(11):1535–44. Available from:
756 https://www.ncbi.nlm.nih.gov/pmc/articles/PMC6158726/

757 30. Xu X, Duan S, Yi F, Ocampo A, Liu GH, Izpisua Belmonte JC. Mitochondrial Regulation in
758 Pluripotent Stem Cells. Cell Metabolism [Internet]. 2013 Sep [cited 2024 Apr
759 29];18(3):325–32. Available from:
760 https://linkinghub.elsevier.com/retrieve/pii/S1550413113002490

761 31. Zhao H, Zhuang Y, Li R, Liu Y, Mei Z, He Z, et al. Effects of different doses of X-ray
762 irradiation on cell apoptosis, cell cycle, DNA damage repair and glycolysis in HeLa cells.
763 Oncol Lett [Internet]. 2019 Jan [cited 2024 May 12];17(1):42–54. Available from:
764 https://www.ncbi.nlm.nih.gov/pmc/articles/PMC6313204/

765 32. Vallabhaneni H, Lynch PJ, Chen G, Park K, Liu Y, Goehe R, et al. High Basal Levels of
766 γH2AX in Human Induced Pluripotent Stem Cells Are Linked to Replication-Associated
767 DNA Damage and Repair. Stem Cells [Internet]. 2018 Oct [cited 2024 May
768 12];36(10):1501–13. Available from:
769 https://www.ncbi.nlm.nih.gov/pmc/articles/PMC6662168/

770 33. Sharma A, Sances S, Workman MJ, Svendsen CN. Multi-lineage Human iPSC-Derived
771 Platforms for Disease Modeling and Drug Discovery. Cell Stem Cell [Internet]. 2020 Mar
772 [cited 2024 May 5];26(3):309–29. Available from:
773 https://linkinghub.elsevier.com/retrieve/pii/S1934590920300643

774 34. Jamieson JJ, Linville RM, Ding YY, Gerecht S, Searson PC. Role of iPSC-derived pericytes
775 on barrier function of iPSC-derived brain microvascular endothelial cells in 2D and 3D.
776 Fluids Barriers CNS [Internet]. 2019 Dec [cited 2020 Sep 15];16(1):15. Available from:
777 https://fluidsbarrierscns.biomedcentral.com/articles/10.1186/s12987-019-0136-7

778 35. Noorani B, Bhalerao A, Raut S, Nozohouri E, Bickel U, Cucullo L. A Quasi-Physiological
779 Microfluidic Blood-Brain Barrier Model for Brain Permeability Studies. Pharmaceutics
780 [Internet]. 2021 Sep 15 [cited 2024 May 12];13(9):1474. Available from:
781 https://www.ncbi.nlm.nih.gov/pmc/articles/PMC8468926/

782 36. Greene C, Hanley N, Campbell M. Claudin-5: gatekeeper of neurological function. Fluids
783 and Barriers of the CNS [Internet]. 2019 Jan 29 [cited 2024 May 13];16(1):3. Available
784 from: https://doi.org/10.1186/s12987-019-0123-z

785 37. Gopinadhan A, Hughes JM, Conroy AL, John CC, Canfield SG, Datta D. A human
786 pluripotent stem cell-derived in vitro model of the blood–brain barrier in cerebral malaria.
787 Fluids Barriers CNS [Internet]. 2024 May 1 [cited 2024 May 13];21(1):38. Available from:
788 https://fluidsbarrierscns.biomedcentral.com/articles/10.1186/s12987-024-00541-9

789 38. Hashimoto Y, Campbell M, Tachibana K, Okada Y, Kondoh M. Claudin-5: A
790 Pharmacological Target to Modify the Permeability of the Blood–Brain Barrier. Biological
791 & Pharmaceutical Bulletin [Internet]. 2021 Oct 1 [cited 2024 May 13];44(10):1380–90.
792 Available from: https://www.jstage.jst.go.jp/article/bpb/44/10/44_b21-00408/_article

793 39. Liu W, Wang Z, Zhang L, Wei X, Li L. Tight Junction in Blood-Brain Barrier: An Overview
794 of Structure, Regulation, and Regulator Substances. CNS Neuroscience & Therapeutics

[Internet]. 2012 Aug [cited 2024 May 13];18(8):609–15. Available from: https://onlinelibrary.wiley.com/doi/10.1111/j.1755-5949.2012.00340.x

Supporting information

S1 Table. Reagents used for cell culture and assays.

S2 Table. Primary antibodies used for immunoassays.

S1 Fig. iM-iPSCs maintained pluripotency through 15 passages in culture. Confocal microscopy images of iPSCs grown from passages 35 to 49 using iMatrix or Matrigel following immunoidentification of pluripotency markers SSEA-4 and OCT-3/4 (red fluorescence) and nuclear staining with DAPI (blue fluorescence). Scale bars: 200 μm. DAPI: 4',6-diamidino-2-phenylindole; OCT-3/4: octamer binding transcription factor-3/4; P: passage; SSEA-4: stage-specific embryonic antigen-4.

S2 Fig. Cryopreservation of iPSC derived brain pericytes. (A) Confocal microscopy images of iM-iPericytes and MG-iPericytes before and after cryopreservation following immunolabeling of PDGFR-β (red fluorescence), NG-2 (green fluorescence), and nuclear staining (blue fluorescence). Scale bars: 200 μm. (B) Phase contrast images of iM-iPericytes frozen with or without rock inhibitor in the freezing media 48 hours after thawing. Scale bars: 500 μm. DAPI: 4',6-diamidino-2-phenylindole; NG-2: neural/glial antigen 2; PDGFR-β: platelet-derived growth factor receptor-β.

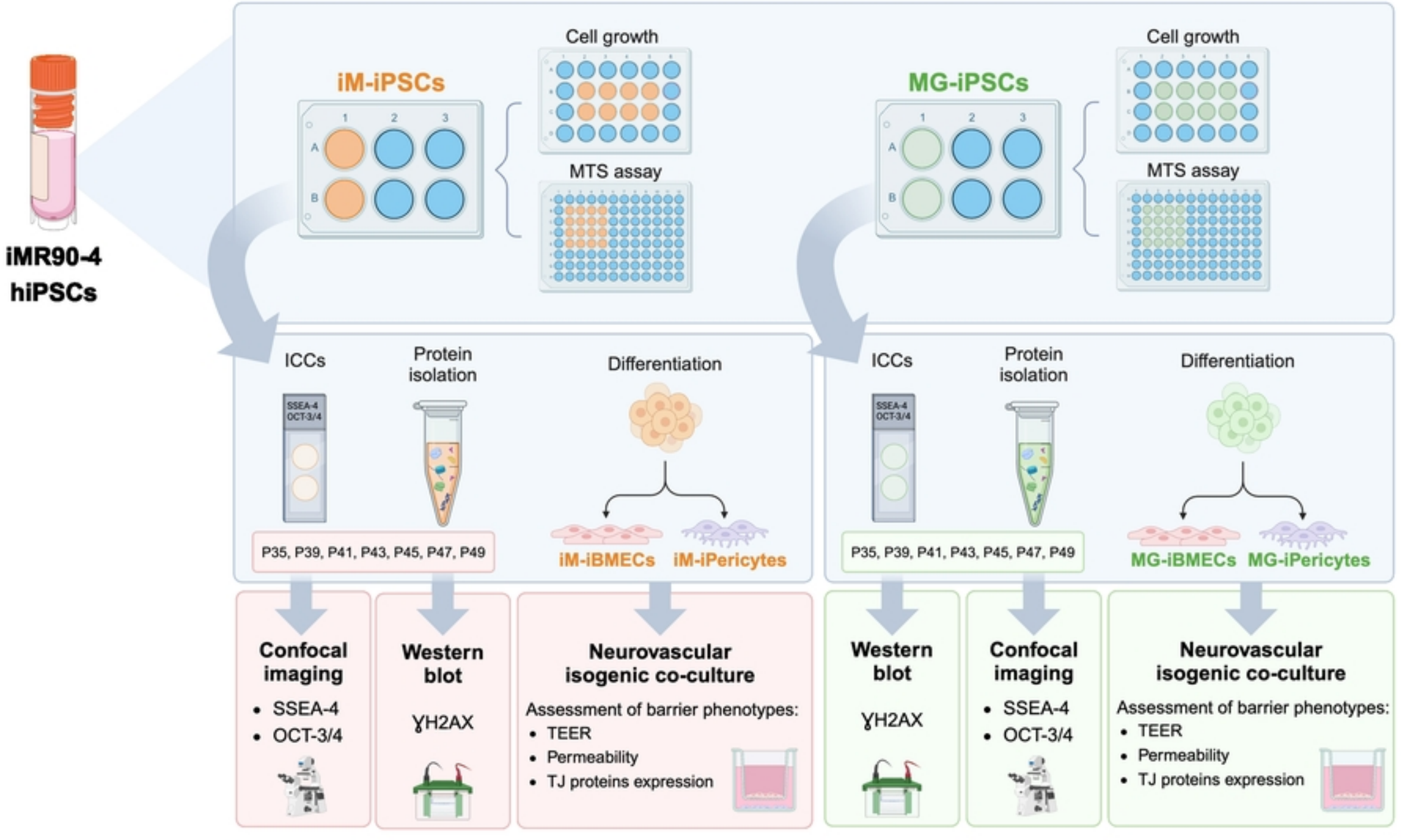
iMR90-4
hiPSCs
iM-iPSCs
Cell growth
MTS assay
MG-iPSCs
Cell growth
MTS assay
ICCs
Protein isolation
Differentiation
SSEA-4
OCT-3/4
P35, P39, P41, P43, P45, P47, P49
iM-iBMECs
iM-iPericytes
ICCs
Protein isolation
Differentiation
SSEA-4
OCT-3/4
P35, P39, P41, P43, P45, P47, P49
MG-iBMECs
MG-iPericytes
Confocal imaging
• SSEA-4
• OCT-3/4
Western blot
γH2AX
Neurovascular isogenic co-culture
Assessment of barrier phenotypes:
• TEER
• Permeability
• TJ proteins expression
Western blot
γH2AX
Confocal imaging
• SSEA-4
• OCT-3/4
Neurovascular isogenic co-culture
Assessment of barrier phenotypes:
• TEER
• Permeability
• TJ proteins expression

Figure 1

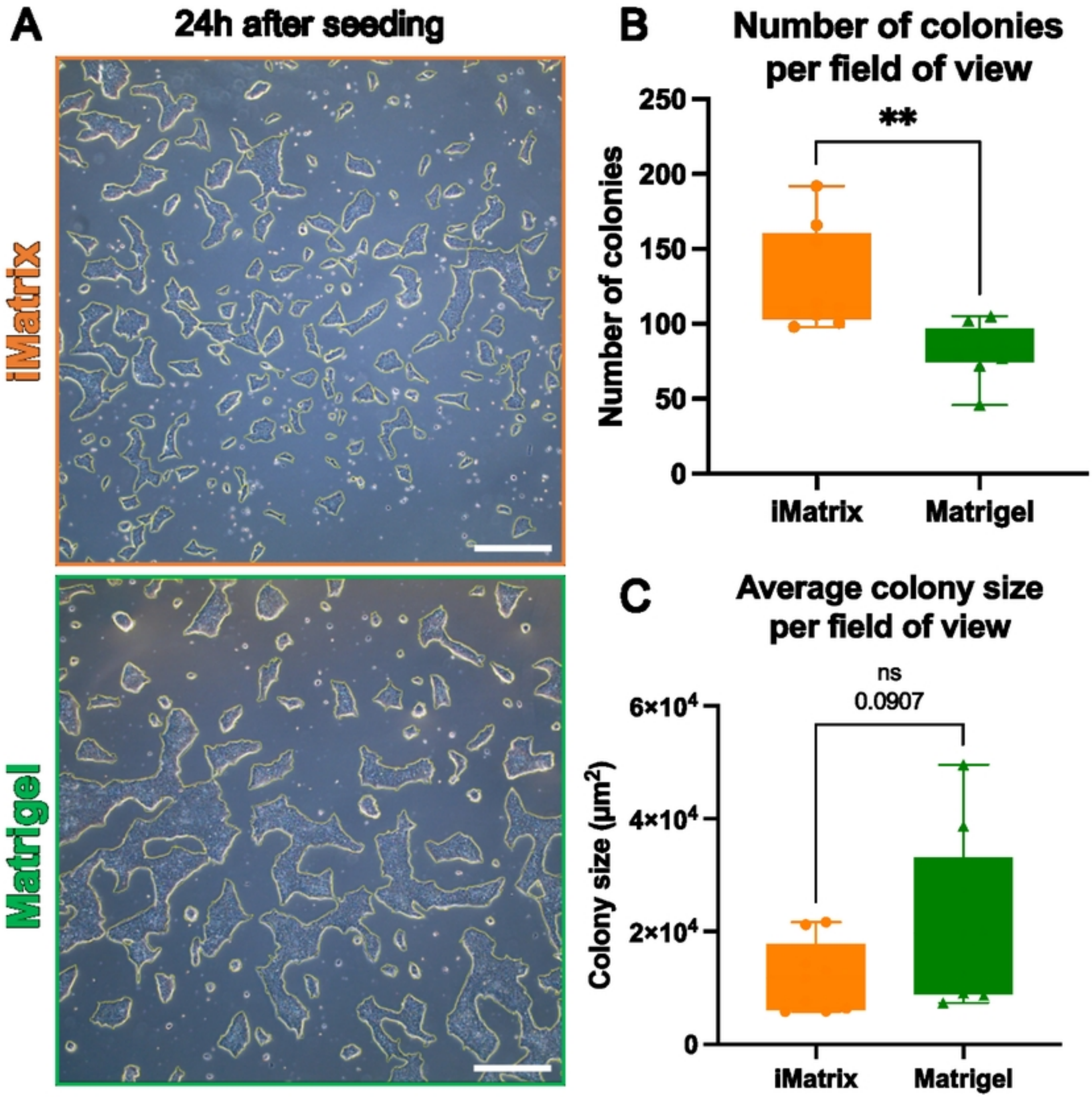
A
24h after seeding
iMatrix
Matrigel
B
Number of colonies per field of view
Number of colonies
250
200
150
100
50
0
**
iMatrix
Matrigel
C
Average colony size per field of view
Colony size (µm²)
6×10⁴
4×10⁴
2×10⁴
0
ns
0.0907
iMatrix
Matrigel

Figure 2

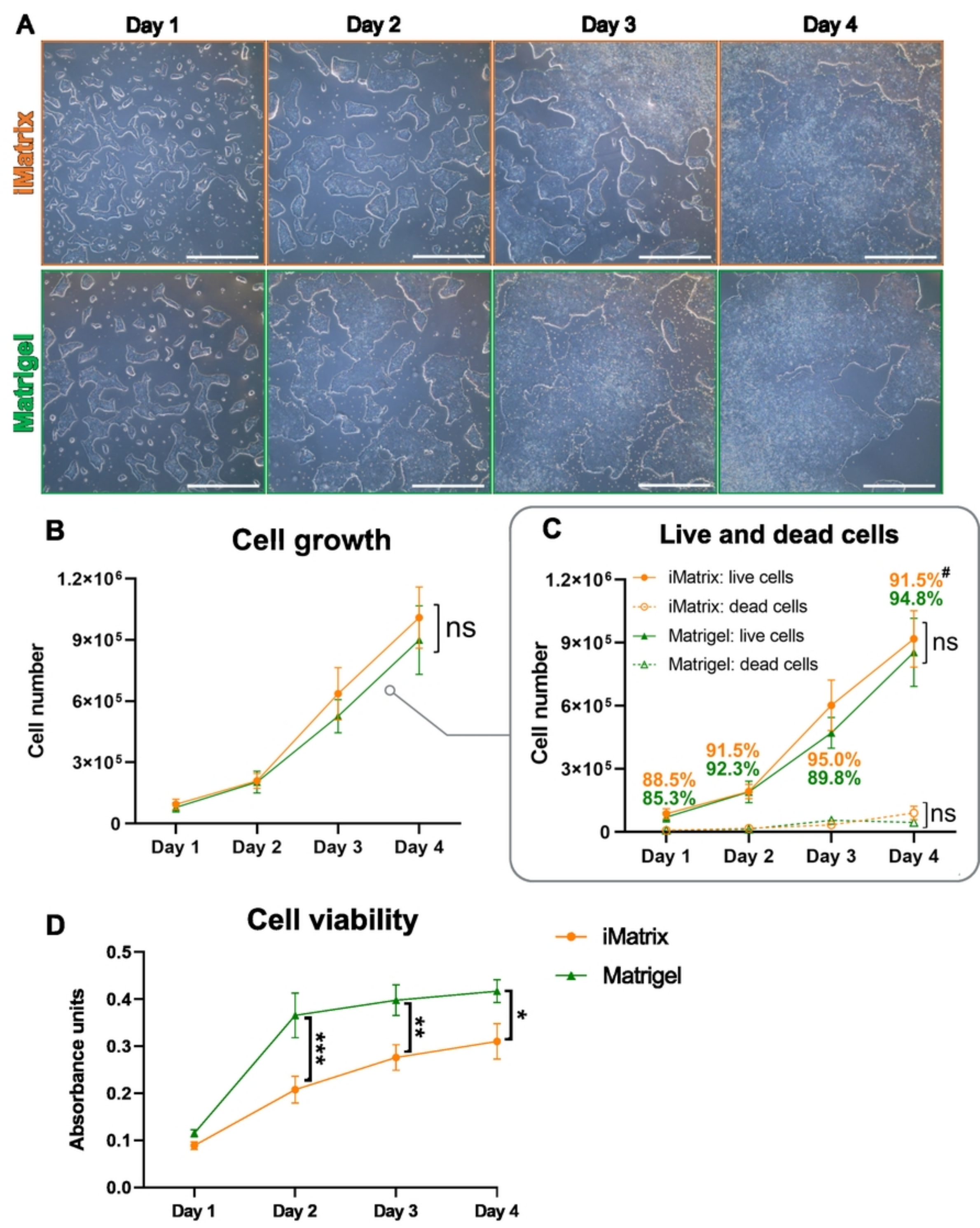
A
Day 1
Day 2
Day 3
Day 4
iMatrix
Matrigel
B
Cell growth
Cell number
1.2×10^6
9×10^5
6×10^5
3×10^5
0
ns
Day 1
Day 2
Day 3
Day 4
C
Live and dead cells
iMatrix: live cells
iMatrix: dead cells
Matrigel: live cells
Matrigel: dead cells
88.5%
85.3%
91.5%
92.3%
95.0%
89.8%
91.5%#
94.8%
ns
ns
D
Cell viability
Absorbance units
0.5
0.4
0.3
0.2
0.1
0.0
***
**
*
iMatrix
Matrigel

Figure 3

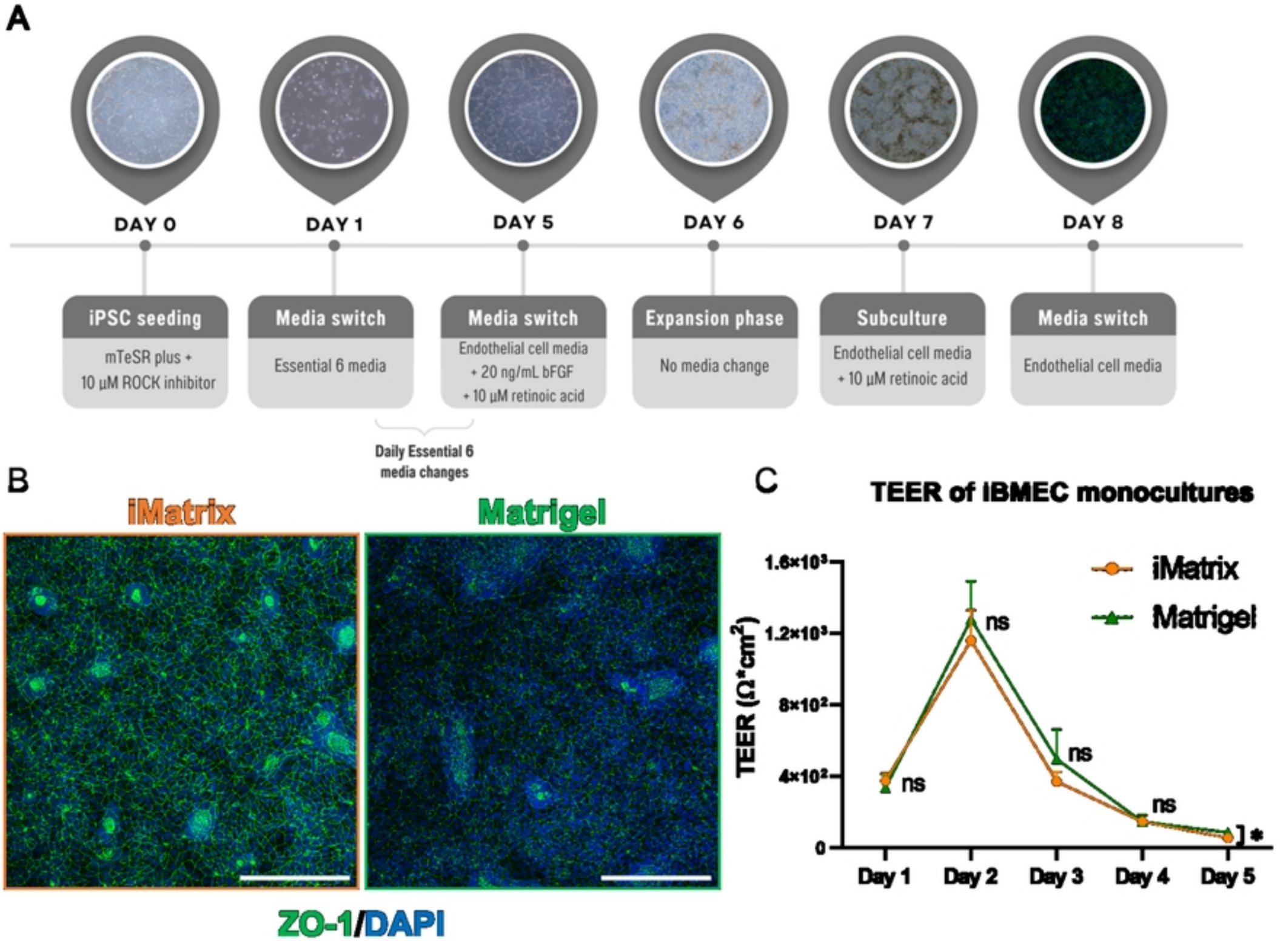
A
DAY 0
DAY 1
DAY 5
DAY 6
DAY 7
DAY 8
iPSC seeding
mTeSR plus + 10 µM ROCK inhibitor
Media switch
Essential 6 media
Media switch
Endothelial cell media + 20 ng/mL bFGF + 10 µM retinoic acid
Expansion phase
No media change
Subculture
Endothelial cell media + 10 µM retinoic acid
Media switch
Endothelial cell media
Daily Essential 6 media changes
B
iMatrix
Matrigel
ZO-1/DAPI
C
TEER of iBMEC monocultures
iMatrix
Matrigel
TEER (Ω*cm²)
1.6×10³
1.2×10³
8×10²
4×10²
0
ns
ns
ns
ns
*
Day 1
Day 2
Day 3
Day 4
Day 5

Figure 5

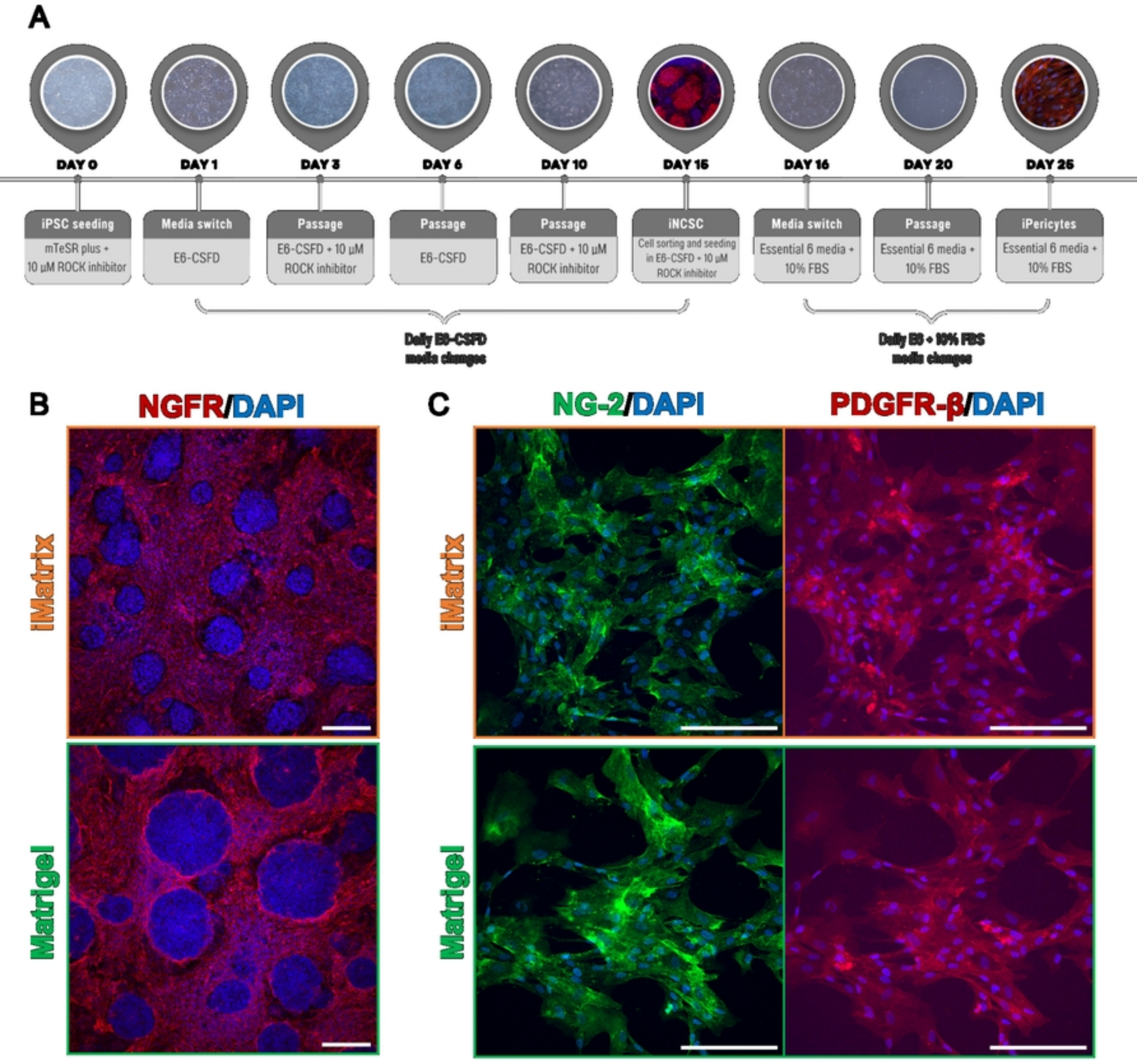
A
DAY 0
DAY 1
DAY 3
DAY 6
DAY 10
DAY 15
DAY 16
DAY 20
DAY 25
iPSC seeding
mTeSR plus + 10 µM ROCK inhibitor
Media switch
E6-CSFD
Passage
E6-CSFD + 10 µM ROCK inhibitor
Passage
E6-CSFD
Passage
E6-CSFD + 10 µM ROCK inhibitor
iNCSC
Cell sorting and seeding in E6-CSFD + 10 µM ROCK inhibitor
Media switch
Essential 6 media + 10% FBS
Passage
Essential 6 media + 10% FBS
iPericytes
Essential 6 media + 10% FBS
Daily E6-CSFD media changes
Daily E6 + 10% FBS media changes
B
NGFR/DAPI
iMatrix
Matrigel
C
NG-2/DAPI
PDGFR-β/DAPI
iMatrix
Matrigel

Figure 6

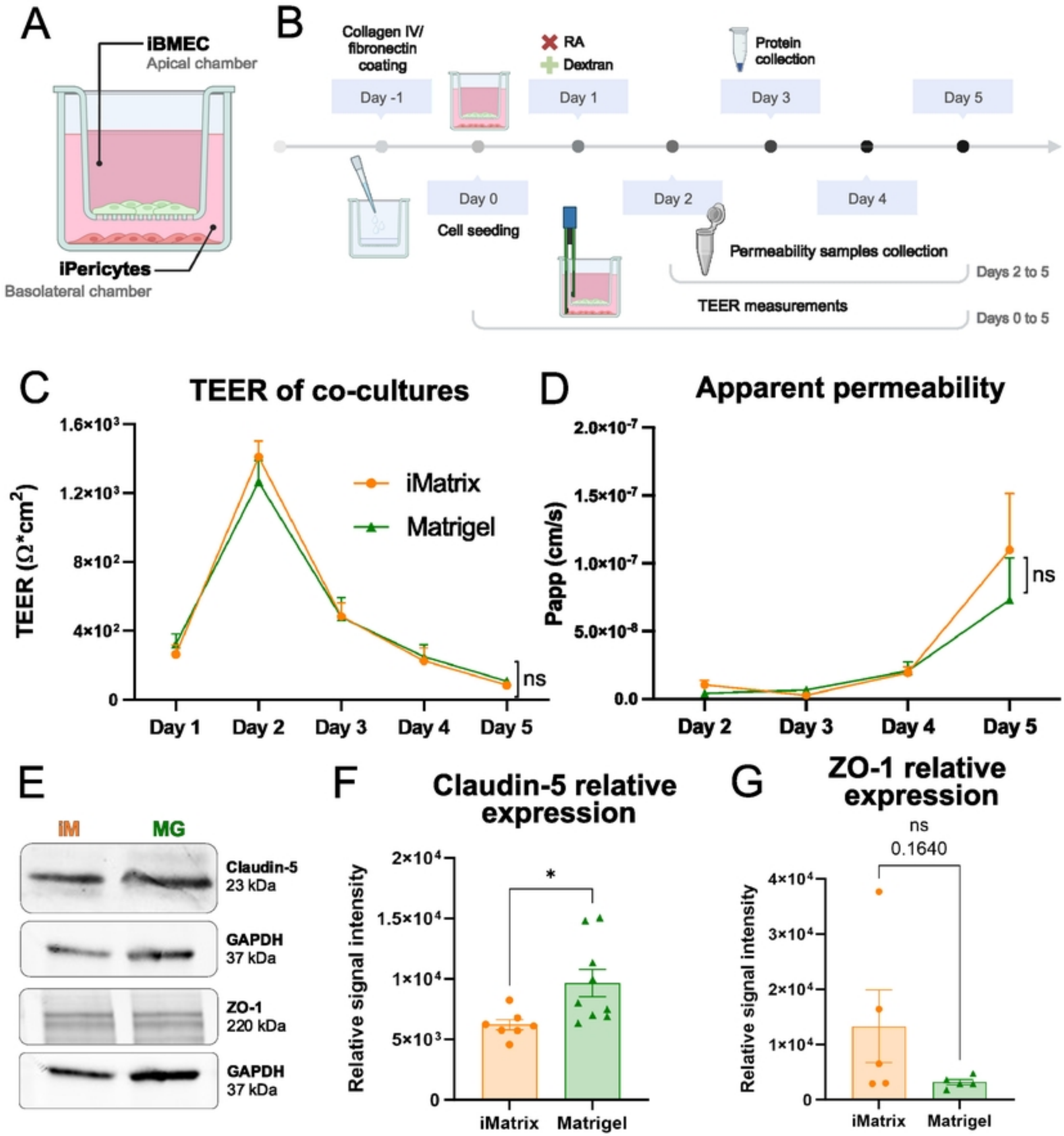
A
iBMEC
Apical chamber
iPericytes
Basolateral chamber
B
Collagen IV/ fibronectin coating
RA
Dextran
Protein collection
Day -1
Day 0
Day 1
Day 2
Day 3
Day 4
Day 5
Cell seeding
Permeability samples collection
TEER measurements
Days 2 to 5
Days 0 to 5
C
TEER of co-cultures
TEER (Ω*cm²)
1.6×10³
1.2×10³
8×10²
4×10²
0
iMatrix
Matrigel
ns
Day 1
Day 2
Day 3
Day 4
Day 5
D
Apparent permeability
Papp (cm/s)
2.0×10⁻⁷
1.5×10⁻⁷
1.0×10⁻⁷
5.0×10⁻⁸
0.0
ns
Day 2
Day 3
Day 4
Day 5
E
IM
MG
Claudin-5
23 kDa
GAPDH
37 kDa
ZO-1
220 kDa
GAPDH
37 kDa
F
Claudin-5 relative expression
Relative signal intensity
2×10⁴
1.5×10⁴
1×10⁴
5×10³
0
*
iMatrix
Matrigel
G
ZO-1 relative expression
ns
0.1640
Relative signal intensity
4×10⁴
3×10⁴
2×10⁴
1×10⁴
0
iMatrix
Matrigel

Figure 7

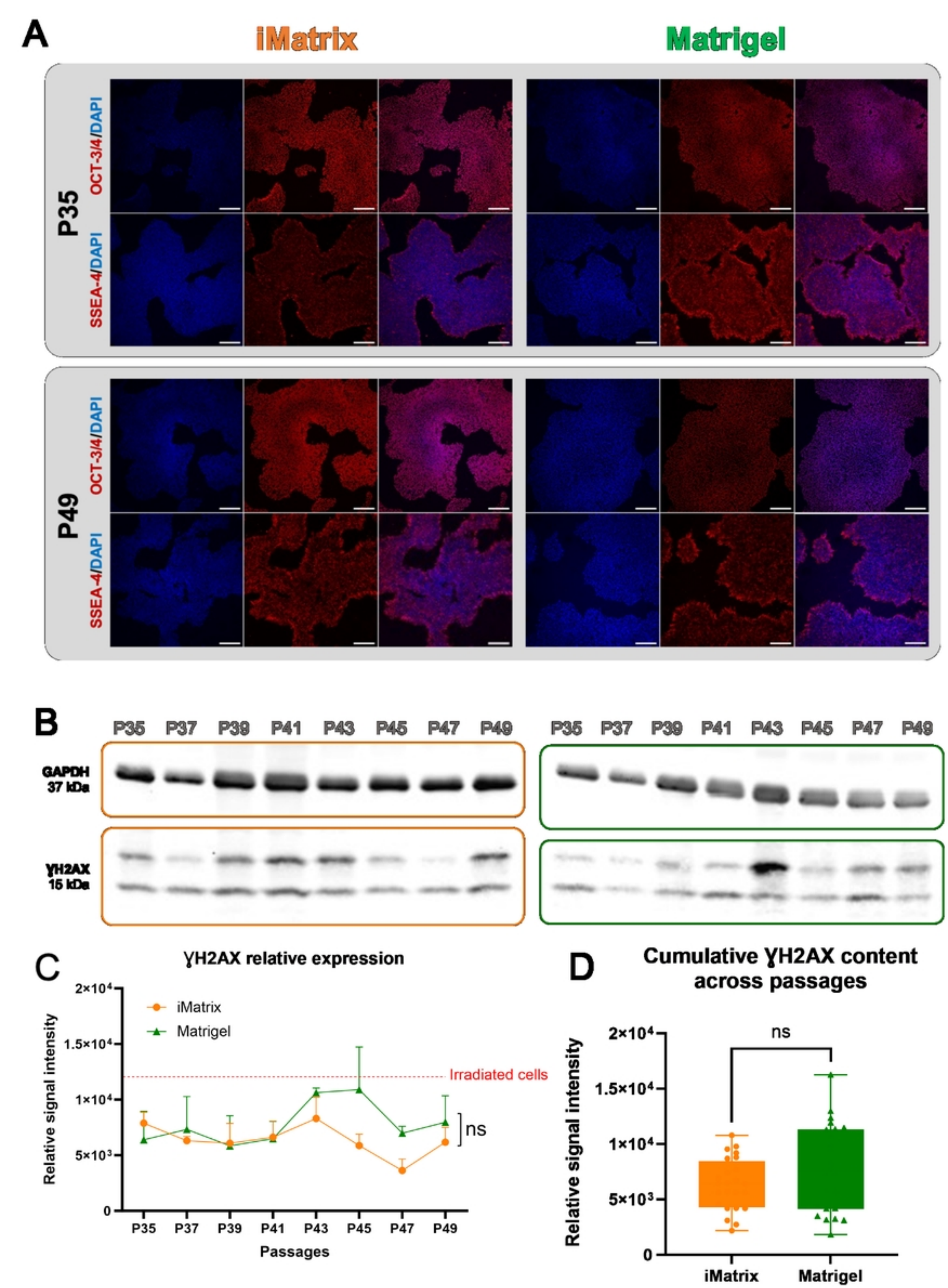
A
iMatrix
Matrigel
P35
OCT-3/4/DAPI
SSEA-4/DAPI
P49
OCT-3/4/DAPI
SSEA-4/DAPI
B
P35 P37 P39 P41 P43 P45 P47 P49
GAPDH
37 kDa
γH2AX
15 kDa
C
γH2AX relative expression
iMatrix
Matrigel
Irradiated cells
ns
Relative signal intensity
2×10⁴
1.5×10⁴
1×10⁴
5×10³
0
Passages
D
Cumulative γH2AX content across passages
ns
Relative signal intensity
iMatrix
Matrigel

Figure 4